

Microwave emissivity of fresh water ice  
–Lake ice and Antarctic ice pack–  
Radiative transfer simulations versus satellite  
radiances.

Peter Mills  
Peteysoft Foundation  
*petey@peteysoft.org*

November 17, 2021

**Abstract**

Microwave emissivity models of sea ice are poorly validated empirically. Typical validation studies involve using averaged or stereotyped profiles of ice parameters against averaged radiance measurements. Measurement sites are rarely matched and even less often point-by-point. Because of saline content, complex permittivity of sea ice is highly variable and difficult to predict. Therefore, to check the validity of a typical, plane-parallel, radiative-transfer-based ice emissivity model, we apply it to fresh water ice instead of salt-water ice. Radiance simulations for lake ice are compared with measurements over Lake Superior from the Advanced Microwave Scanning Radiometer on EOS (AMSR-E). AMSR-E measurements are also collected over Antarctic icepack. For each pixel, a thermodynamic model is driven by four years of European Center for Medium Range Weather Forecasts (ECMWF) reanalysis data and the resulting temperature profiles used to drive the emissivity model. The results suggest that the relatively simple emissivity model is a good fit to the data. Both cases, however, show large discrepancies whose most likely explanation is scattering both within the ice sheet as well as by cloudy atmospheres. Scattering is neglected by the model. Further work is needed to refine the scattering component of ice emissivity models and to generate accurate estimates of complex permittivities within sea ice.

# 1 Introduction

In Mills and Heygster (2011b), a plane-parallel radiative transfer (RT) model was used to simulate emitted microwave brightness temperatures at L-band (1.4 GHz) frequencies. The question addressed in this paper is simply the following: is such a model a reasonable approximation to reality? Can factors not accounted for in the model, such as ice ridging and surface scattering, be neglected? The results of Mills and Heygster (2011b) suggest that while the effect of ice ridging is small, it is not insignificant.

Because of the simplicity of the model and because effective permittivities, required as input to the model, are notoriously difficult to estimate for saline ice (Ulaby et al., 1986; Mills and Heygster, 2011b), such a model would be a good candidate for inverse methods that aim to retrieve physical properties of sea ice beyond mere concentration. The idea is to retrieve those quantities most relevant to the model, namely the complex permittivities, rather than going one step further back and trying to retrieve ice bulk and microstructural properties. The model is only appropriate to lower (below 25 GHz) frequencies where volume scattering is weak (Mills and Heygster, 2011b; Barber et al., 1998; Vant et al., 1978; Stogryn, 1986; Johnsen, 1998). The functional dependence of permittivity with frequency in this range also tends to be weak (Vant et al., 1978), thus it may be possible to assume constant permittivity across all frequencies.

With the launch of the new SMOS instrument operating at L-band, the possibilities for such a retrieval expand considerably. With SMOS, there is some potential to retrieve ice thickness. In the event that ice is too opaque for this, however, another good candidate for retrieval is snow-thickness. Dry snow is nearly transparent at L-band but becomes progressively more opaque at higher frequencies (see Equation (4)).

The motivation for this study is two-fold: first, there is a near absence of direct, point-by-point validation studies of ice emissivity models of this type, that is, by taking ice cores, feeding the measured profiles into an emissivity model and comparing the results to radiance measurements taken at corresponding locations. Most validation studies consist of comparing averaged measured brightness temperatures with simulations based on averaged or idealized vertical ice profiles. Second, the complex permittivity of pure ice is much less variable than that of saline ice, making it easier to predict. Because of the very low value of the imaginary part, which determines the attenuation, the effect of ice thickness on the signal over thin ice, i.e., over lake ice, will be relatively small.

The procedure will be to simulate microwave emission over freshwater

ice— Lake Superior and the Antarctic ice cap—and compare these with satellite measurements from the Advanced Microwave Scanning Radiometer on EOS (AMSR-E).

## 2 Models

### 2.1 Emissivity model

The radiative transfer model used here is described thoroughly in Mills and Heygster (2011b) so only the briefest treatment will be given here. A plane parallel geometry is assumed making it possible to solve for upwelling and downwelling radiances along a single line-of-sight:

$$T_i \uparrow - \tau_i(1 - R_i)T_{i+1} \uparrow - \tau_i R_i T_i \downarrow = (1 - \tau_i)T_i \quad (1)$$

$$T_i \downarrow - \tau_i(1 - R_{i-1})T_{i-1} \downarrow - \tau_i R_{i-1} T_i \uparrow = (1 - \tau_i)T_i, \quad (2)$$

where  $T_i$  is the physical temperature of the  $i$ th layer,  $T_i \uparrow$  and  $T_i \downarrow$  are the upwelling and downwelling radiances (as brightness temperatures) respectively. If there are discontinuous interfaces between the layers, the reflection coefficients,  $R_i$  can be calculated from the Fresnel equations. The transmission coefficients,  $\tau_i$ , is derived:

$$\tau_i = \exp\left(-\frac{\alpha_i \Delta z_i}{\cos \theta_i}\right), \quad (3)$$

from the layer thickness,  $\Delta z$ , the transmission angle,  $\theta_i$  (calculated from Snell's law), and the attenuation coefficient,  $\alpha_i$ :

$$\alpha_i = \frac{4\pi\nu}{c} \text{imag} n_i, \quad (4)$$

which, in turn, depends on the frequency,  $\nu$  and the imaginary part of the refractive index,  $n_i = \sqrt{\epsilon_i}$ .  $c$  is the speed of light and  $\epsilon_i$  is the relative permittivity.

To run the model, we will need relative permittivities as input. The real part for pure ice tends to be fairly constant at around 3.15. The following, temperature-dependent model is given in Maetzler (2006):

$$\epsilon'_{pi} = 3.1884 + 9.1 \times 10^{-4}T \quad (5)$$

where  $T$  is the physical temperature in degrees Celsius. Ice is almost a perfect dielectric: the imaginary permittivity at microwave frequencies is very

small, generally less than 0.01. We use the model from Hufford (1991) to model the imaginary permittivity of pure ice as a function of temperature and frequency. These estimates will suffice for lake ice, however the density of ice pack in the Antarctic varies between less than 500 kg/m<sup>3</sup> at the surface to over 900 kg/m<sup>3</sup> or close to the density of pure ice, at tens of metres depth. Since the ice pack is typically granular, we use a mixture model for spherical inclusions to calculate the effective permittivity (Sihvola and au Kong, 1988):

$$\epsilon^* = \epsilon_1 + \frac{3f(\epsilon_2 - \epsilon_1)\epsilon_1/(\epsilon_1 + 2\epsilon_2)}{1 - f(\epsilon_2 - \epsilon_1)/(\epsilon_2 + \epsilon_1)} \quad (6)$$

where  $\epsilon_1$  is the complex permittivity of pure ice,  $\epsilon_2 = 1$  is the permittivity of air and  $f = 1 - \rho/\rho_{pi}$  is the relative volume of air, which we can calculate from the density of the snowpack,  $\rho$ , versus the density of pure ice,  $\rho_{pi}$ .

We use the following exponential model from Rist et al. (2002) for the density of snowpack as a function of depth:

$$\rho = 918. - 539. \exp(-z/32.5) \quad (7)$$

where  $z$  is depth.

## 2.2 Thermodynamic model

For the 6GHz channel, the most important determinant of the microwave signature of Antarctic ice pack is the temperature and our results will show this. For higher frequencies, the temperature becomes less important, but is still nonetheless significant. Because of the high penetration depth of low-frequency microwaves in pure ice, temperatures quite deep in the ice will affect the signal. They will also vary quite significantly from those on the surface because of thermal conduction lag. Thermal conduction is modelled in one dimension with the diffusion equation:

$$\frac{\partial T}{\partial t} = \frac{\rho_0 \kappa}{\rho C_p} \frac{\partial^2 T}{\partial z^2} \quad (8)$$

where  $\kappa$  is the thermal conductivity of ice,  $C_p$  is its heat capacity and  $\rho_0$  its maximum density. The top layer is forced from European Centre for Medium Range Forecasts (ECMWF) fields of surface air temperature,  $T_a$ , surface wind speed,  $v$ , humidity,  $q$ , and cloud-cover,  $c$ . These are used to determine the surface heat flux,  $Q^*$ , which is a sum of the four components of the flux:

$$Q^* = Q_{SW}(t, \phi, c) + Q_{LW}(T_a^4, T_0^4, c) + Q_E(e_s(T_a), e_s(T_0), v) + Q_H(T_a, T_0, v) \quad (9)$$

which are, from left to right: shortwave, longwave, latent and sensible. The functional dependencies for typical parameterizations are given (see, for instance Yu and Lindsay (2003));  $T_0$  is the surface temperature and  $e_s$  is the saturation vapour pressure. The shortwave flux is calculated primarily from geometrical considerations. The local solar zenith angle is calculated as follows:

$$\beta = \cos^{-1} \left( \frac{\cos \phi \cos \theta \cos \lambda - \sin \phi \cos \delta \sin \lambda}{\sqrt{\cos^2 \delta \sin^2 \lambda + \cos^2 \lambda}} \right) \quad (10)$$

where  $\phi$  is the latitude,  $\lambda$  is the Earth's tilt,  $\theta$  is the time of day as an angle (angle of rotation of the Earth around its axis) with  $\theta = 0$  representing noon while  $\theta = \pi$  is midnight,  $\delta$  is the day of the year (angle of revolution about the sun) with  $\delta = 0$  being the winter solstice.

To return the flux, we multiply the cosine of the local solar zenith angle with the solar “constant,”  $S$ , the cloud cover and the albedo,  $a$ :

$$Q_{SW} = S \cos \beta (1 - 0.62c)(1 - a) \quad (11)$$

Spatial derivative were calculated using finite-differencing while the equation was integrated in time with a fourth-order Runge Kutta (Press et al., 1992). The simulation was initialized with a linear temperature profile, starting at freezing at the bottom 300 m which was used as the fixed boundary condition (Rist et al., 2002). It was then spun up by repeated forcing with four years of National Center for Environmental Prediction (NCEP) reanalysis data.

### 2.3 Atmospheric model

To correct for atmospheric influences we use the parametrised model from Wentz and Meissner (2000); Wentz (1997). In the Wentz-Meissner model, atmospheric transmissivity and atmospheric components of upwelling and downwelling radiation are derived from column water-vapour and cloud water path based on fitted polynomials. The upwelling and downwelling brightness temperatures are modelled as equivalent temperatures assuming an isothermal atmosphere.

The total downwelling radiation from the atmosphere will be given as follows:

$$T_{ba} \downarrow = (1 - \tau_a)T_d + \tau T_{bsky} \quad (12)$$

where  $\tau_a$  is the atmospheric transmissivity,  $T_d$  is the equivalent atmospheric temperature for the downwelling case and  $T_{bsky}$  is the cosmic background

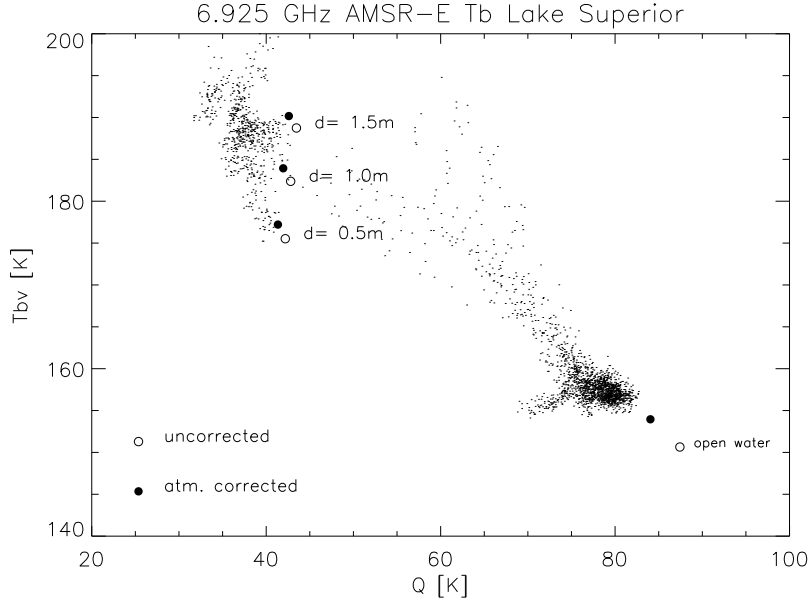


Figure 1: AMSR-E brightness temperatures at 6 GHz over Lake Superior during the winter of 2003. Dots are measured, circles are model results, both uncorrected (open) and corrected for atmospheric influences (open circles).

radiation. The upwelling radiation will be given as:

$$T_{ba} \uparrow = \tau_a T_1 \uparrow + (1 - \tau) T_u \quad (13)$$

where  $T_1 \uparrow$  is the modelled surface brightness temperature from the solution of Equations (1) and (2) and  $T_u$  is the equivalent atmospheric temperature for the upwelling case. If the upwelling and downwelling temperatures are equal,  $T_d = T_u$ , (they are typically very close) then we can model the atmosphere by simply adding an extra layer (the atmosphere) to the ice RT model (1) and (2) and setting the topmost reflection coefficient (interface between the atmosphere and space) to zero.

### 3 Results

#### 3.1 Simulation of lake ice

AMSR-E measurements were collected over the middle of Lake Superior (in a radius of 20 km from the coordinate 87 degrees E longitude and 48 degrees N

Table 1: Table of atmospheric correction coefficients calculated according to Wentz and Meissner (2000). See Equations (12) and (13) for their use. Column water vapour was set at 20 kg/m<sup>2</sup> and cloud water path at 0.1 mm.

$\nu$ [GHz]	$\tau_a$	$T_u$ [K]	$T_d$ [K]
6.925	0.981	260.7	260.9
10.65	0.974	262.5	262.6
18.70	0.911	268.8	269.3

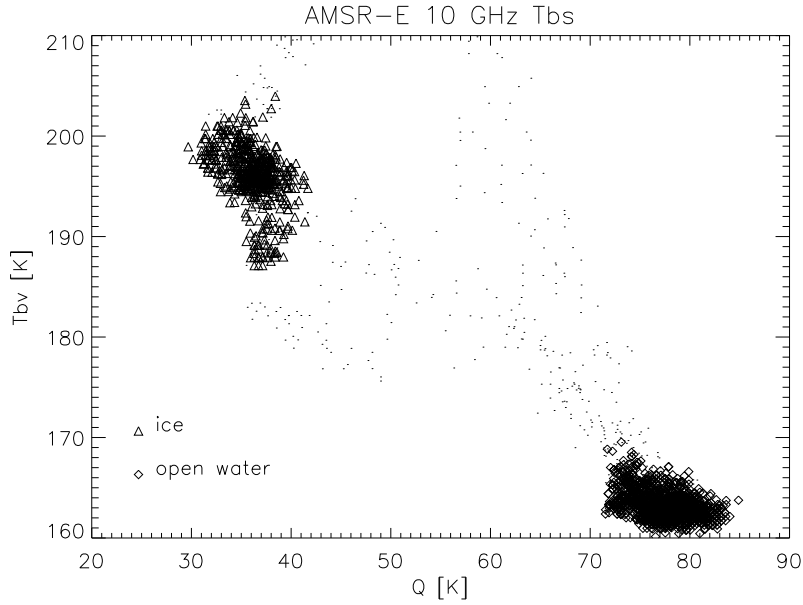


Figure 2: Measured AMSR-E brightness temperatures at 10 GHz over Lake Superior during the winter of 2003. A clustering algorithm has been used to separate lake ice from open water points, with the triangles being ice and the diamonds open water.

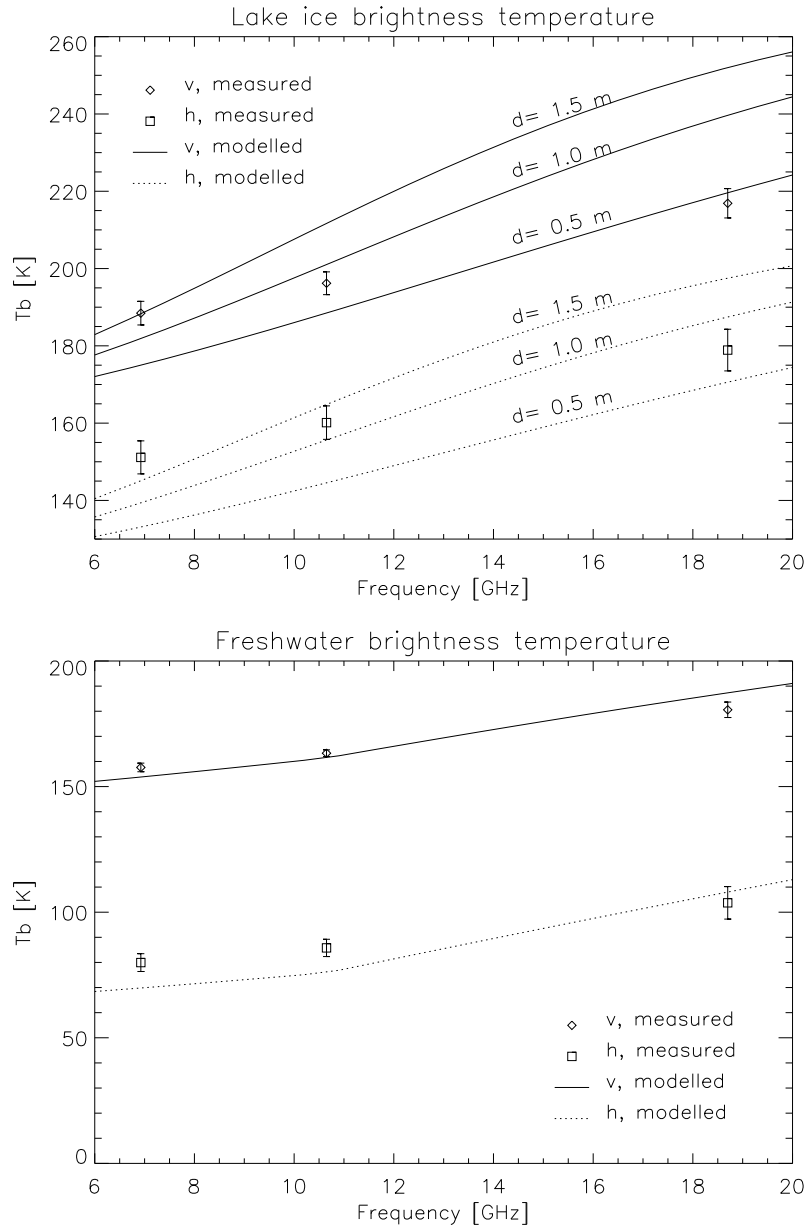


Figure 3: AMSR-E brightness temperatures over Lake Superior during the winter of 2003. Lines show model results while points with error bars are measured. Top is ice, bottom is open water.



latitude) for the winter of 2003 during which there was much lake ice. These are compared with brightness temperature simulations for the 6 GHz case in Figure 1. A constant ice temperature of zero degrees Celsius was assumed. The water temperature was likewise assumed constant at freezing and its complex permittivity modelled with a Debye relaxation curve (Ulaby et al., 1986).

Measured and modelled values are compared in a brightness temperature space consisting of the vertically polarised brightness temperature versus the polarisation difference. The cluster of dots on the bottom right is open water while the cluster on the top left is lake ice while the larger circles are the model results, both corrected for atmospheric effects and uncorrected. Correction coefficients are shown in Table 1, calculated according to Wentz and Meissner (2000) assuming total column water vapour of 20 kg/m<sup>2</sup> and an ice water path of 0.1 mm.

Simulations are performed for three different ice thicknesses. Fresh water ice is almost a perfect dielectric – because of the low value of the imaginary part of the permittivity, ice thickness will have less of an effect on the final, emitted brightness temperature. Since it is lake ice, we expect it to be relatively thin, certainly less than 2 m.

We use a clustering algorithm based on kernel density estimation (Michie et al., 1994; Terrell and Scott, 1992; Mills, 2009) to group the open water and ice points and separate the two classes from one another as demonstrated in Figure 2. Averages for each cluster, along with tolerances calculated from the standard deviations are plotted as a function of frequency in Figure 3 along with model results.

### 3.2 Simulation of Antarctic icepack

Icepack simulations are a bit more involved because the density of the ice varies with depth and because we have to model the internal temperature using the thermodynamic model described in Section 2.2. 5000 measurements were chosen at random from AMSR-E swath data in a broad area between 0 and 120 degrees East longitude 75 and 85 degrees South latitude for the year of 2007. A thermodynamic model forced by four years of NCEP data was run for each of the points and then fed to the radiative transfer model. A sample temperature profile is shown in Figure 4. Results are shown in Figures 5 through 7.

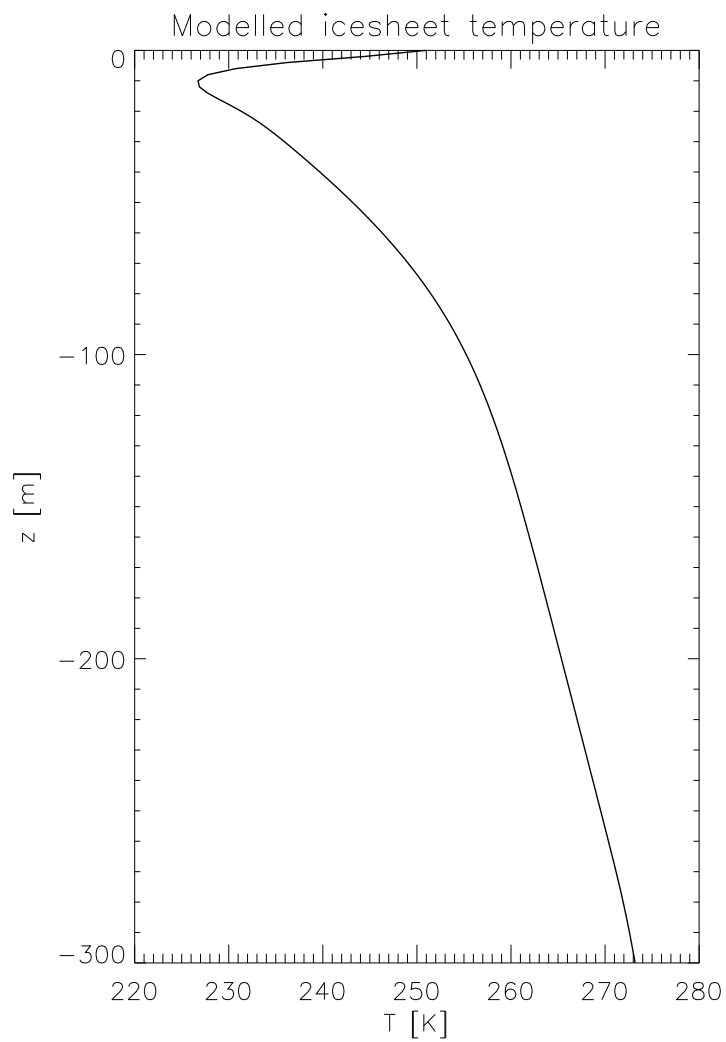


Figure 4: Antarctic ice sheet temperature profile for 27 November 2007, 14:42:41 UT at  $102.97^\circ$  E,  $76.60^\circ$  S. Profile has been modelled from four years of NCEP reanalysis data using a thermodynamic model.

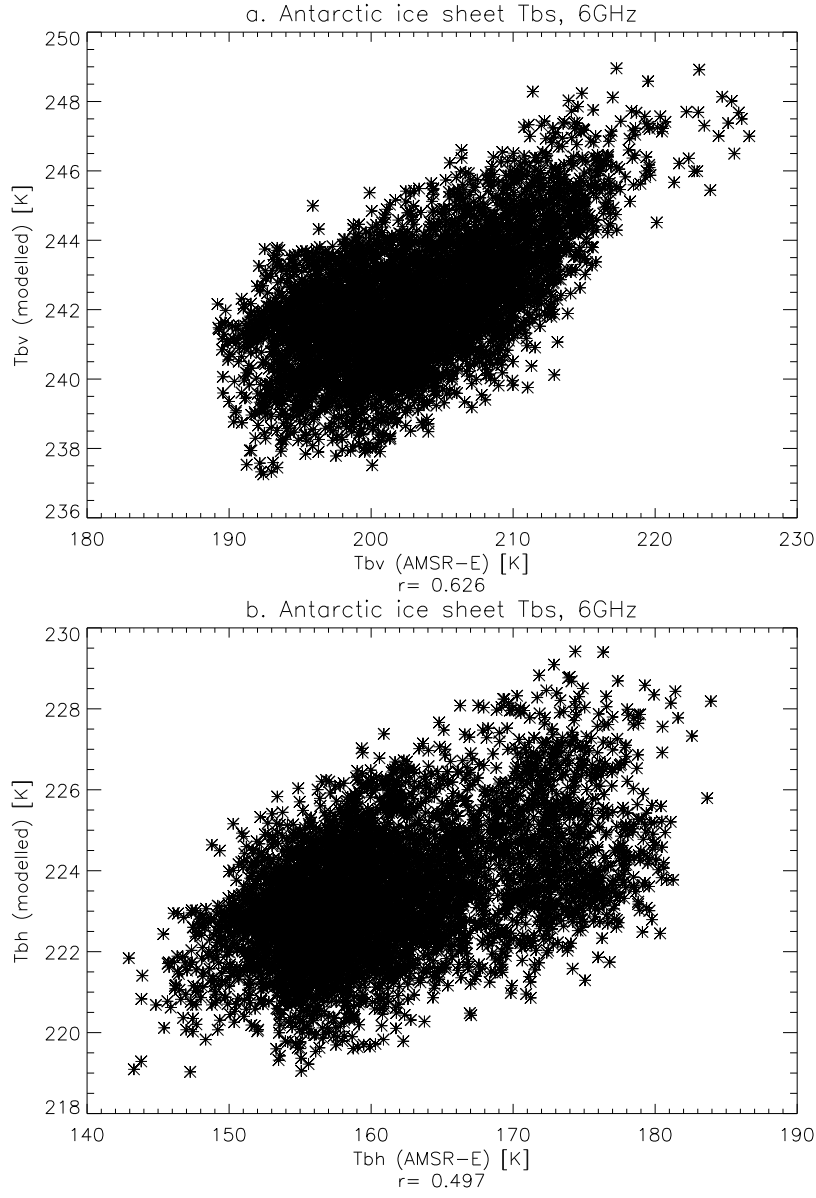


Figure 5: Radiative transfer simulations of AMSR-E brightness temperatures over Antarctic ice pack for the 6 GHz channel.

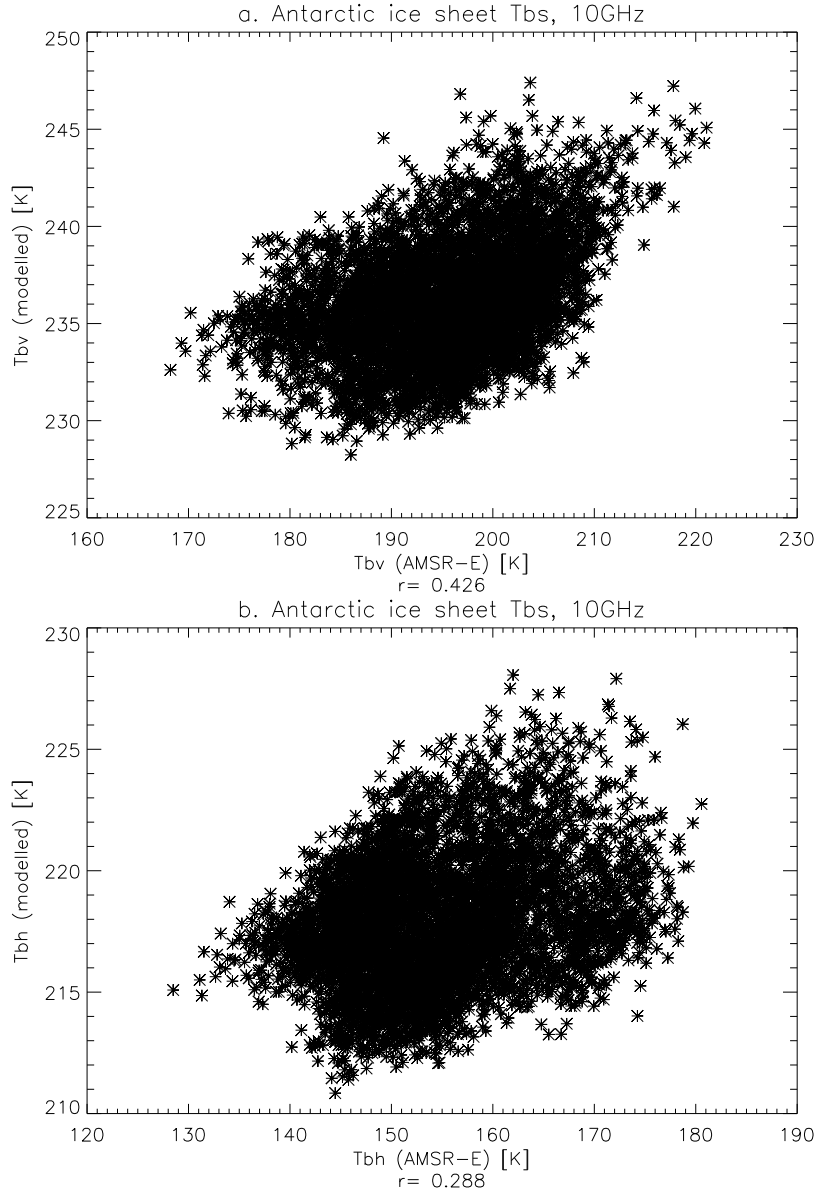


Figure 6: Radiative transfer simulations of AMSR-E brightness temperatures over Antarctic ice pack for the 10 GHz channel.

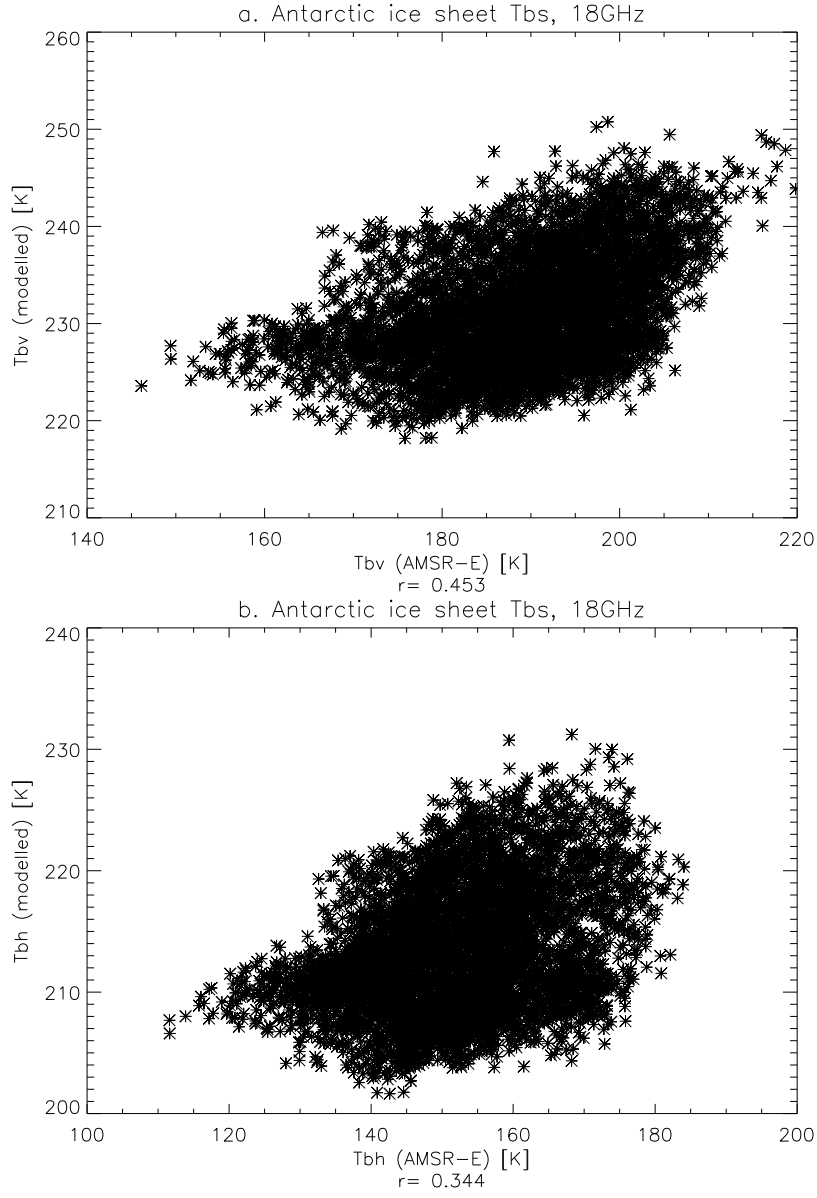


Figure 7: Radiative transfer simulations of AMSR-E brightness temperatures over Antarctic ice pack for the 18 GHz channel.

## 4 Discussion and conclusions

The plane-parallel radiative transfer model is able to simulate radiance measurements from the AMSR-E satellite instrument well, but with large bias. For the case of lake ice, brightness temperatures are under-estimated for the 6 GHz channels, slightly over-estimated for the 10 GHz vertical channel slightly under-estimated for the 10 GHz horizontal channel and badly over-estimated for the 18 GHz channels, especially in the vertical polarization. For higher-frequencies channels, discrepancies are easily accounted for by the lack of scattering in the model. As you move up the microwave spectrum from low to high frequency, simple absorption and reflection processes become less and less important, while scattering begins to dominate. The tendency of scattering, especially within the ice sheet (as opposed to surface scattering) is to lower the emissivity along with a complementary increase in the polarization difference. Indeed, the measured signal shows an increase in the polarization difference which is absent from the modelled signal. In fact, the polarization difference over the ice is larger for the measured signal over all frequencies. This may be accounted for in part by the presence of clouds which were not screened for when selecting measurement pixels.

Similar discrepancies show up in the open-water signal. In addition to scattering caused by clouds and rough surface conditions, the difference may also be caused by water temperatures above freezing as the temperature of the lake-water was not varied. Sadly, these are still not point-by-point validations and with only six data points provide only weak validation of the plane-parallel RT model. Recently, Kang et al. (2010) have derived ice thickness from AMSR-E measurements over the Great Bear and Great Slave Lakes. This is a statistical model, however, so it would be good to confirm the relationship based on more physical considerations, hopefully paving the way for more physically-based ice retrieval methods over the ocean, just as exist for retrieval of atmospheric parameters. Preliminary results suggest that, except for melting ice, the RT model does an excellent job of predicting AMSR-E radiances based strictly on thickness. As in the current work, ice temperature was held constant. Since the lake ice thicknesses in Kang et al. (2010) were generated using a thermodynamic ice growth model, temperatures within the ice sheet were returned as a by-product. The author hopes to publish a more complete study using these to drive the emissivity model.

For a truly point-by-point analysis, we turn to the model of Antarctic icepack. Here the magnitudes are far off, with the model severely over-estimating the actual values, however the correlation, while not excellent,

Table 2: Biases of the radiative transfer emissivity model compared with AMSR-E data over Antarctic icepack. Linear-regression slope and offset parameters are presented for all six channels.

Channel	Slope	Bias
6v	0.180	-39.2
6h	0.106	-62.2
10v	0.157	-40.7
10h	0.086	-63.3
18v	0.239	-42.3
18h	0.148	-61.4

is nonetheless strong and significant. As before, the bias is easily explained by scattering as glacial icepack tends to be very granular with grain sizes as large as 15 mm (Rist et al., 2002). Thus scattering will strongly affect even the lowest, 6 GHz channel. Biases are shown in Table 2 which lists regression slope and offset values for all six channels. As expected, biases are different for the vertical versus horizontal channels in keeping with the scattering explanation. Considering that the only input parameters varied in the emissivity model were the temperatures, and these were derived indirectly from a thermal conductivity model driven by reanalysis data, the results seem quite good.

It is instructive to compare the RT results with a purely statistical model. Therefore, 1000 temperature profiles were selected for use as “training data” and correlated with the AMSR-E brightness temperatures using the top ten (10) singular vectors. Predicted brightness temperatures for the other 4000 measurement pixels are presented in Figures 8 through 10 along with AMSR-E brightness temperatures for comparison. Although the large biases are absent, the results are remarkable both for the similarities in accuracy as well as in the shape of the scatterplots. This is hardly surprising since the RT model is practically linear, with the only non-linearities arising from the weak dependence of real permittivity on temperature.

The weighting coefficients for the RT versus statistical model are compared in Figure 11(a) and 11(b). For the statistical model, simulated brightness temperatures are simply a linear combination of the temperatures of the icepack. To account for the weak nonlinearity in the RT model, weights are calculated with a numerical derivative,  $\frac{\partial T_b}{\partial T_i}$ , averaged over 500 trials: standard deviations are also shown in the figures.

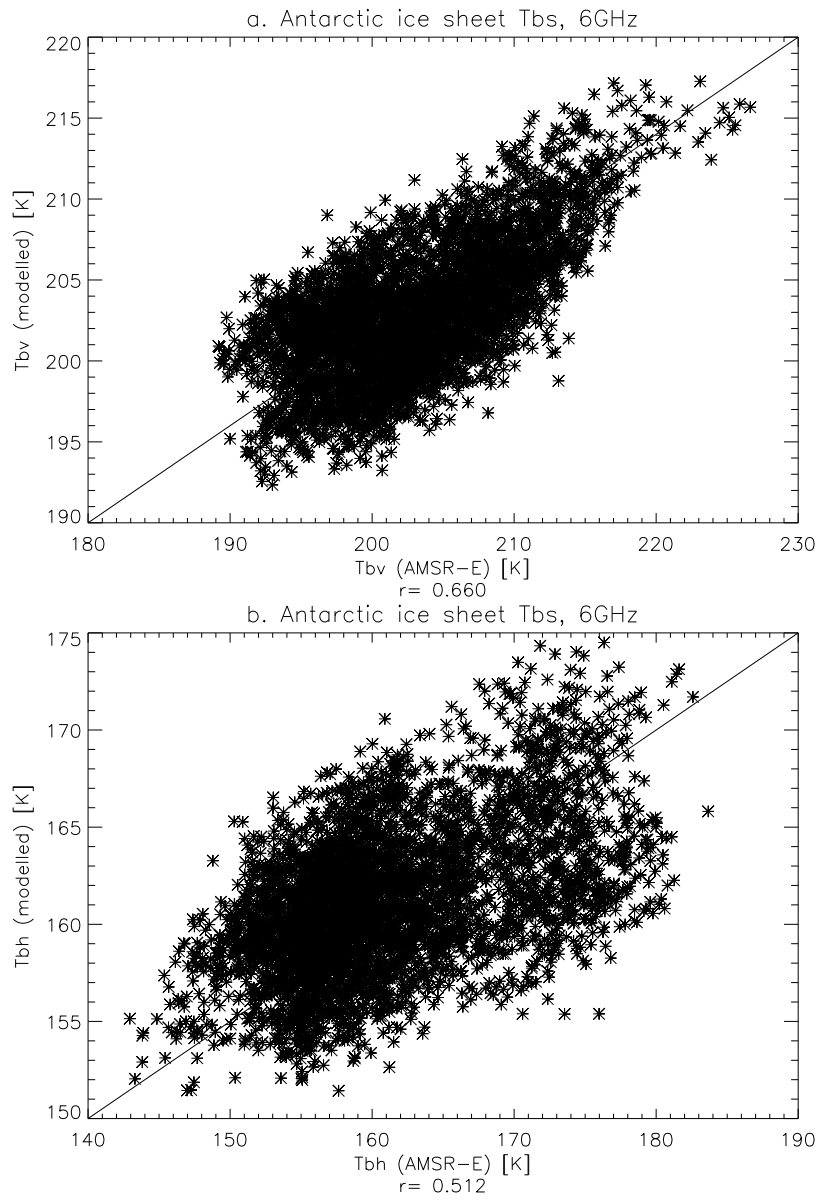


Figure 8: Statistical model of AMSR-E brightness temperatures over Antarctic ice pack for the 6 GHz channel.



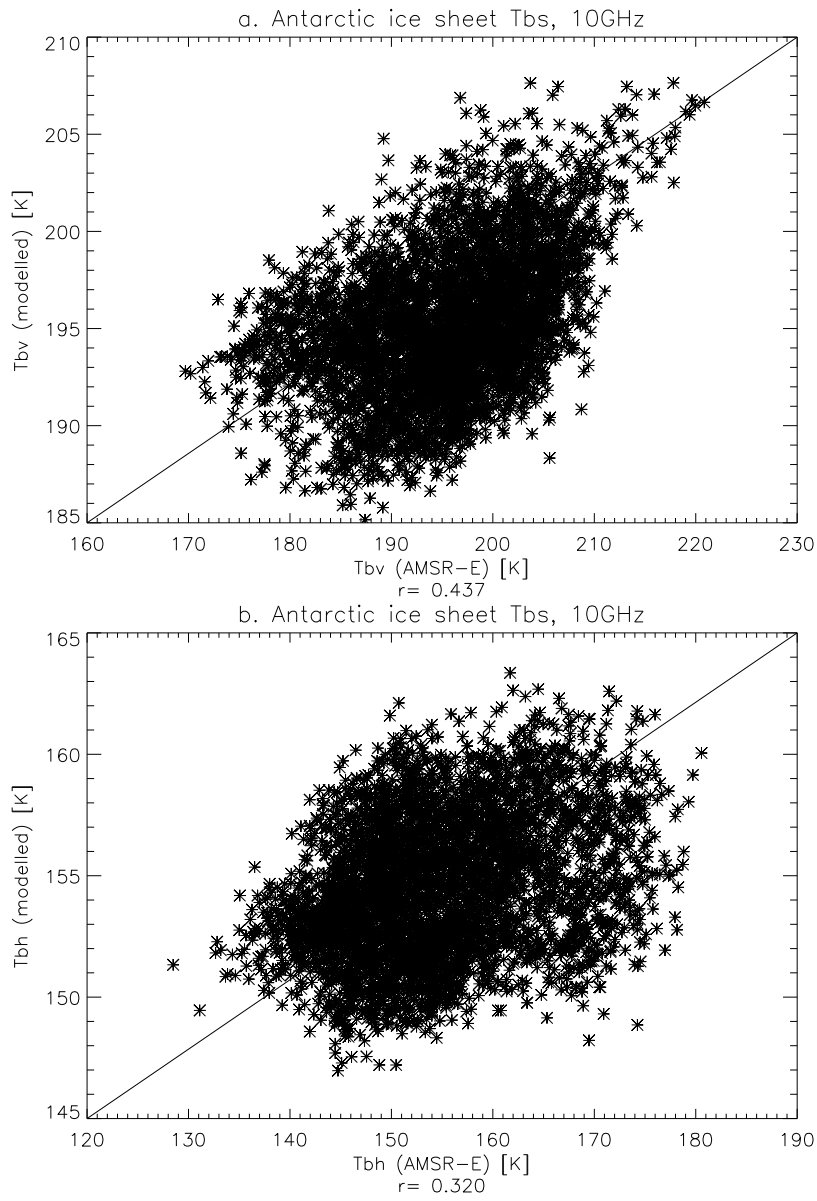


Figure 9: Statistical model of AMSR-E brightness temperatures over Antarctic ice pack for the 10 GHz channel.

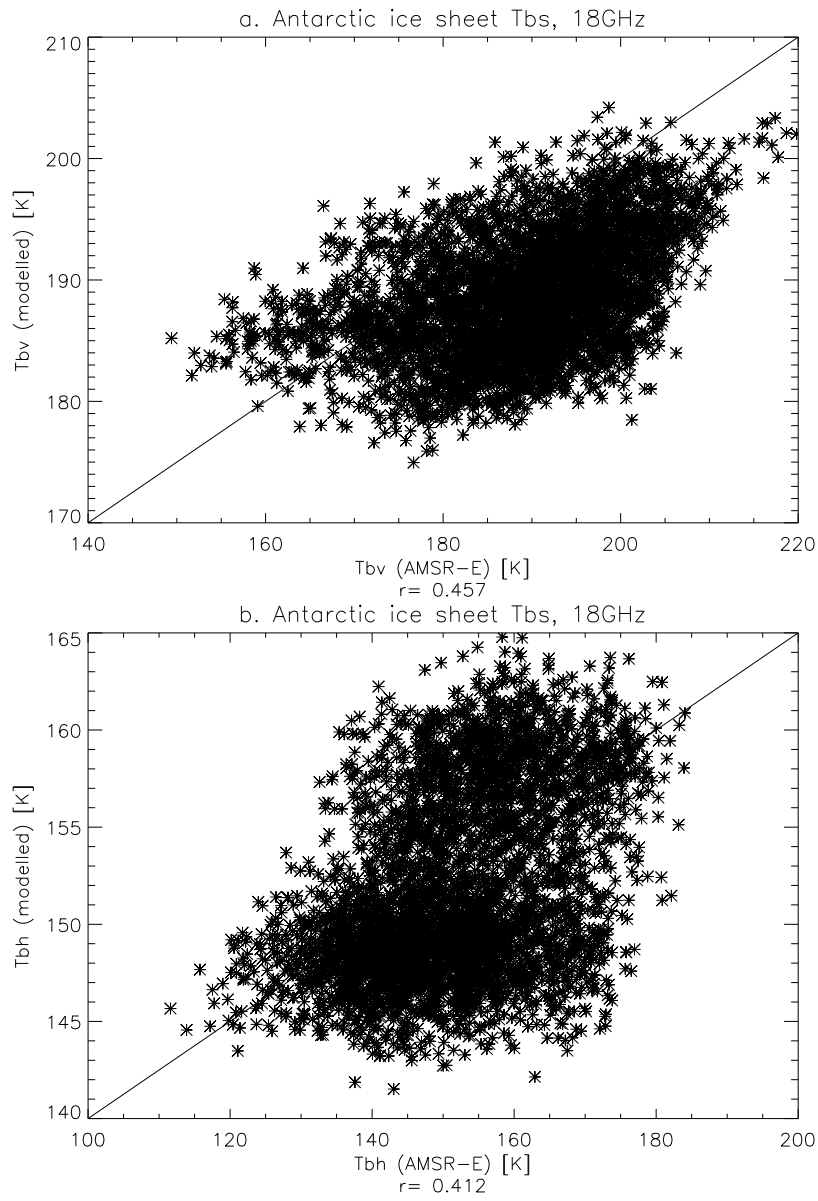


Figure 10: Statistical model of AMSR-E brightness temperatures over Antarctic ice pack for the 18 GHz channel.

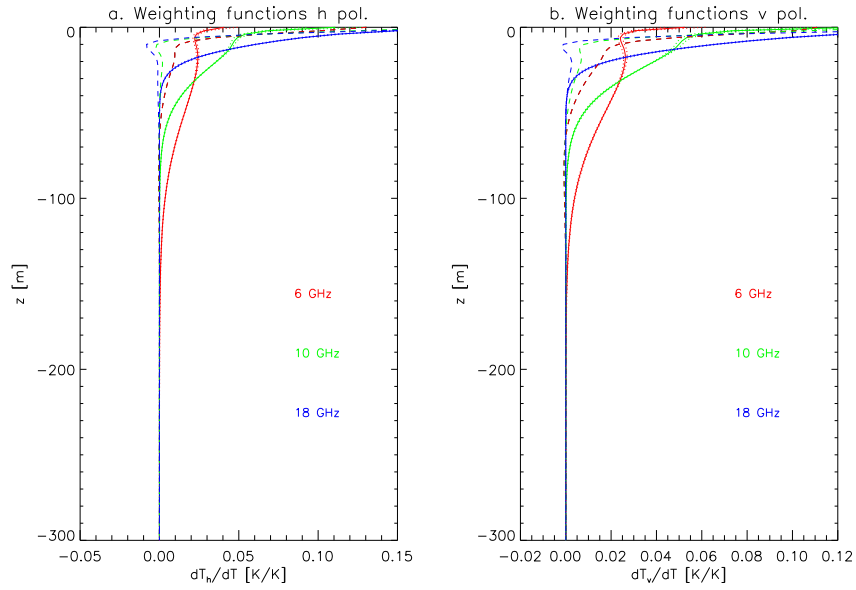


Figure 11: Temperature weighting functions for Antarctic ice sheet for horizontal (a) and vertical polarizations (b). The weighting functions for the radiative transfer simulations represent an average over fifty (50) AMSR-E measurement pixels randomly selected from the test set. The averages are shown by the solid line while the dotted lines enclose the standard deviations. The broken lines show the weighting coefficients for the statistical model.

The two types of weighting functions are quite similar, although the statistical weighting functions are shifted considerably upwards. They also allow for negative weight. Thus, scattering means that the ice pack is effectively much more opaque than our non-scattering model suggests. This provides a further explanation for the too-high brightness temperatures returned by the RT model since ice temperatures tend to be higher further down in the icepack—see Figure 4. Nonetheless, the penetration depth of the microwaves is quite deep: as much as 50 m for the lowest frequency. This means that radiometer measurements of glacial icepack return information about temperatures within the ice sheet, which are reflective of historical temperature.

The interaction of electro-magnetic radiation with matter is a very fundamental problem. Most operational ice retrieval algorithms are based primarily on empirical parameterizations. While the model under discussion is somewhat ad-hoc, nonetheless it is based on real physics. Such physical models are invaluable for ice retrieval efforts, both for use as forward models and to retrieve physical characteristics of ice sheets. Most likely parameters to be retrieved include ice temperature, ice thickness and in particular, complex permittivities within the ice sheet which are reflective of the ice composition and micro-structural properties. Retrieving fresh-water ice thickness appears to be quite easy, however retrieving salt-water ice thickness is proving to be quite difficult (Mills and Heygster, 2011b,a).

Ice, particularly saline ice, is a highly complex composite. Because of this complexity, determining its electromagnetic properties—how it interacts with radiation—is very difficult. More work needs to be done to understand how ice emits, absorbs and scatters electromagnetic radiation.

## References

- Barber, D. G., Fung, A. K., Grenfell, T. C., Nghiem, S. V., Onstott, R. G., Lytle, V. I., Perovich, D. K., and Gow, A. J. (1998). The Role of Snow on Microwave Emission and Scattering over First-Year Sea Ice. *IEEE Transactions on Geoscience and Remote Sensing*, 36(5):1750–1763.
- Hufford, G. (1991). A model for the complex permittivity of ice at frequencies below 1 THz. *International Journal of Infrared and Millimeter Waves*, 12(7):677–682.
- Johnsen, K.-P. (1998). *Radiometrische Messungen im arktischen Ozean—*

- Vergleich von Theorie und Experiment.* PhD thesis, Universitaet Bremen, Otto-Hahn Allee 1, Bremen, Germany.
- Kang, K.-K., Duguay, C. R., Howell, S. E. L., Derksen, C. P., and Kelly, R. E. J. (2010). Sensitivity of AMSR-E Brightness Temperature to the Seasonal Evolution of Lake Ice Thickness. *IEEE Geoscience and Remote Sensing Letters*, 7(4):751–755.
- Maetzler, C., editor (2006). *Thermal Microwave Radiation: Applications for Remote Sensing*. The Institution of Engineering and Technology.
- Michie, D., Spiegelhalter, D. J., and Tayler, C. C., editors (1994). *Machine Learning, Neural and Statistical Classification*. Ellis Horwood Series in Artificial Intelligence. Prentice Hall, Upper Saddle River, NJ.
- Mills, P. (2009). Isoline retrieval: An optimal method for validation of advected contours. *Computers & Geosciences*, 35(10):2020–2031.
- Mills, P. and Heygster, G. (2011a). Sea ice brightness temperature as a function of ice thickness: Computed curves for AMSR-E and SMOS (frequencies from 1.4 to 89 GHz). Technical Report DFG project HE-1746-15, University of Bremen.
- Mills, P. and Heygster, G. (2011b). Sea ice emissivity at L-band and application to Pol-Ice campaign field data. *IEEE Transactions on Geoscience and Remote Sensing*, 49(2):612–627.
- Press, W. H., Teukolsky, S. A., Vetterling, W. T., and Flannery, B. P. (1992). *Numerical Recipes in C*. Cambridge University Press, second edition.
- Rist, M. A., Sammonds, P. R., Oerter, H., and Doake, C. S. M. (2002). Fracture of Antarctic shelf ice. *Journal of Geophysical Research*, 107(B1).
- Sihvola, A. H. and au Kong, J. (1988). Effective Permittivity of Dielectric Mixtures. *IEEE Transactions on Geoscience and Remote Sensing*, 26(4).
- Stogryn, A. (1986). A Study of Microwave Brightness Temperatures of Snow from the Point of View of Strong Fluctuation Theory. *IEEE Transactions on Geoscience and Remote Sensing*, GE-24(2):220–231.
- Terrell, D. G. and Scott, D. W. (1992). Variable kernel density estimation. *Annals of Statistics*, 20:1236–1265.

- Ulaby, F. T., Moore, R. K., and Fung, A. K., editors (1986). *Microwave Remote Sensing: Active and Passive, Volume III, From Theory to Applications*. Artech House, Norwood, MA.
- Vant, M. R., Ramseier, R. O., and Makios, V. (1978). The complex-dielectric constant of sea ice at frequencies in the range 0.1-40 ghz. *Journal of Applied Physics*, 49(3):1264–1280.
- Wentz, F. J. (1997). A well-calibrated ocean algorithm for Special Sensor Microwave/Imager. *Journal of Geophysical Research*, 107(C4):8703–8718.
- Wentz, F. J. and Meissner, T. (2000). AMSR Ocean Algorithm. Algorithm Theoretical Basis Document RSS Tech. Proposal 121599A-1, Remote Sensing Systems, Santa Rosa CA. prepared for NASA Goddard.
- Yu, Y. and Lindsay, R. W. (2003). Comparison of thin ice thickness derived from RADARSAT Geophysical Processor System and Advanced Very High Resolution Radiometer data sets. *Journal of Geophysical Research*, 108(C12).